Research Article

Noble gas geochemistry of phenocrysts from the Ciomadul volcanic dome field (Eastern Carpathians)

Kata Molnár [a,b,*], György Czuppon [a,c], László Palcsu [a], Zsolt Benkó [a], Réka Lukács [d], Boglárka-Mercédesz Kis [a,d,e], Bianca Németh [b,d], Szabolcs Harangi [b,d]

[a] Isotope Climatology and Environmental Research Centre, Institute for Nuclear Research, Bem tér 18/c, Debrecen H-4026, Hungary
[b] Department of Petrology and Geochemistry, Eötvös Loránd University, Pázmány Péter stny, 1/c, Budapest H-1117, Hungary
[c] Institute for Geological and Geochemical Research, Research Centre for Astronomy and Earth Sciences, Eötvös Loránd Research Network, Budaörsi út 45, Budapest H-1112, Hungary
[d] MTA-ELTE Volcanology Research Group, Pázmány Péter stny. 1/c, Budapest H-1117, Hungary
[e] Faculty of Biology and Geology, Babeş-Bolyai University, Str. Mihail Kogălniceanu 1, Cluj-Napoca, Romania

ARTICLE INFO

ABSTRACT

Noble gas isotopic composition of fluid inclusions was analyzed in amphibole, plagioclase and clinopyroxene phenocrysts from the shoshonitic and dacitic volcanic products of the Ciomadul volcanic dome field, the youngest volcanic system within the Carpathian-Pannonian Region. The highest R$_c$/R$_A$ ratios (3.0–3.8 R$_A$) were obtained for high-mg clinopyroxene of the Malnaş shoshonite. High-Al amphiboles from the Bixad dacitic pumices have R$_c$/R$_A$ ratios between 1.16 and 2.11 R$_A$. These values overlap with the noble gas signature of the present-day CO$_2$ emission. Thus, our new results reinforce the conclusion that the mantle component of the Ciomadul primitive magmas has relatively lower R$_c$/R$_A$ signature compared to the nearby Perşani lithospheric mantle. This is likely due to the thorough metasomatic nature resulting in elevated large ion lithophile elements and high water content of the Ciomadul magmas. On the other hand, the R$_c$/R$_A$ ratios from plagioclase-hosted fluid inclusions and those from low-Al amphiboles are 0.06–0.12 R$_A$ and 0.39–0.77 R$_A$, respectively defining a dominant crustal origin (>90%) for the trapped fluids. Noteworthy, these minerals represent a low-temperature crystal mush assemblage that existed for protracted time in the magma reservoir. We tested the fraction of mantle contribution for different mantle end-member values, considering also the effect of magma aging on the R/R$_A$ ratios due to longer (up to 50 kyr) residence time. This resulted in a maximum of ~50–60% mantle fluid contribution for the high-Al amphibole-hosted fluid inclusions and a lower, ~25% mantle fluid contribution, for the low-Al amphiboles. The elevated mantle fluid contribution in the case of the high-Al amphiboles can be explained by a fresh magma recharge event and shorter residence time before the eruption. The results of this study imply that fluid inclusion in primitive clinopyroxene and amphibole phenocrysts could reflect the magmatic end-member, which is in the case of Ciomadul a strongly metasomatized lithospheric mantle with relatively low R$_c$/R$_A$ values. Thus, the noble gas signature of the lithospheric mantle could be heterogeneous even in a restricted area.

© 2021 Published by Elsevier B.V.

1. Introduction

Elemental and isotopic composition of noble gases from free gases, water samples and fluid inclusions of different mineral phases can reveal important information about the origin of the fluids from which they formed, since different geochemical reservoirs (e.g., crust, mantle and air) have distinct noble gas signatures (Ozima and Podosek, 2004). Therefore, noble gas isotopes are often used in volcanic systems to constrain the origin of hot springs, fumaroles and bubbling pools (e.g., Caracausi et al., 2003, 2013; Daskalopoulou et al., 2018; Kis et al., 2017, 2019; Paonita et al., 2012; Sano et al., 2015). In addition, noble gas elemental and isotopic compositions of phenocryst-hosted inclusions in volcanic rocks can help to constrain the origin and evolution of the magma and better understand the magmatic processes within the lithosphere (e.g., Battaglia et al., 2018; Martelli et al., 2004; Marty et al., 1994; Rizzo et al., 2015; Robidoux et al., 2020). The noble gases typically partition into CO$_2$-rich fluids, which form the most common type of mantle fluid inclusions (Dunai and Porcelli, 2002). Olivine, clino- and orthopyroxene are the most widely used mineral phases (Hilton et al., 2002), occurring as phenocrysts either in volcanic rocks or xenoliths although, amphibole, plagioclase and leucite were also used as host minerals to trace mantle fluids and magmatic processes (e.g. Althaus et al., 1998; Correale et al., 2019; Graham et al., 1993; Hanyu and Kaneoka, 1997).

* Corresponding author at: Isotope Climatology and Environmental Research Centre, Institute for Nuclear Research, Bem tér 18/c, Debrecen H-4026, Hungary.
E-mail address: molnar.kata@atomki.hu (K. Molnár).

The shoshonitic to dacitic Ciomadul volcanic dome field (CVDF) is the youngest volcanic system in eastern-central Europe, the last eruption occurring at ca. 30 ka (Harangi et al., 2010, 2015a, 2020; Molnár et al., 2019), and it is characterized by significant present-day CO_2 emission occurring as dry mofettes, bubbling pools and CO_2 bubbling peat bogs (Jánosi et al., 2011; Kis et al., 2017; Vaselli et al., 2002). The noble gas signatures of these gas discharges revealed the presence of a deeper, mantle-derived component (Althaus et al., 2000; Kis et al., 2019; Vaselli et al., 2002). Magnetotelluric and petrologic studies suggested that melt-bearing magma body could still exist in the crust beneath the volcano (Harangi et al., 2015b; Laumonier et al., 2019) and therefore the potential for future reactivation cannot be excluded. A recent study on the shoshonites (Bracco Gartner et al., 2020) implies that the primary magmas derived from a strongly metasomatized lithospheric mantle, which is consistent with the enrichment of large ion lithophile elements (e.g. Ba, Sr) in the erupted products (Molnár et al., 2018, 2019). In addition to Ciomadul, Pleistocene volcanism occurred in this area at the alkaline basaltic Perşani volcanic field at 1.2–0.6 Ma (PVF; Panaiotu et al., 2013). The basaltic magma has an asthenospheric origin (Bracco Gartner et al., 2020; Downes et al., 1995; Harangi et al., 2013), but carried a vast amount of ultramafic xenoliths from the lithospheric mantle (Vaselli et al., 1995; Falus et al., 2008; Faccini et al., 2020).

This study aims to better constrain the pristine noble gas composition of the Ciomadul magma and compare it to the present-day outgassing source. For this purpose, we analyzed various phenocrysts from the shoshonites and dacites of Ciomadul. We performed He, Ne and Ar measurements on plagioclase and amphibole phenocrysts of dacitic pumice samples from the youngest eruption period (ca. 56–30 ka; Molnár et al., 2019) and on high-mg clinopyroxene separates from the Malnaş shoshonitic lava rock, which marks the onset of the CVDF activity at ca. 1 Ma (Molnár et al., 2018) representing the most primitive phase of the volcanic system. The data were compared with the noble

gas isotopic signatures of the present-day CO_2 gas emissions and those obtained for the mineral phases of the ultramafic xenoliths of Perşani (Althaus et al., 1998; Kis et al., 2019; Faccini et al., 2020; this study). With only few reported studies of amphibole noble gas composition (e.g. Correale et al., 2019; Hanyu and Kaneoka, 1997), our detailed study extends the application of amphibole in the understanding of noble gas systematics of volcanic systems.

2. Geological and volcanological background

The Ciomadul volcanic dome field (CVDF) is situated at the southeastern end of the andesitic-dacitic Călimani-Gurghiu-Harghita volcanic chain in the Eastern Carpathians (Romania; Fig. 1; Szakács et al., 2015). This post-collisional volcanic chain extends over ~160 km, and is characterized by a gradual shift of the locations and ages of the eruption centers towards the southeast (e.g., Pécskay et al., 1995, 2006; Seghedi et al., 2004, 2011, 2019; Szakács and Seghedi, 1995). This is coupled with a gradual decrease in eruptive volumes and a compositional shift towards more potassic, incompatible element-enriched eruptive products (Dibacto et al., 2020; Harangi and Lenkey, 2007; Karátson and Tímár, 2005; Mason et al., 1996; Molnár et al., 2018, 2019; Seghedi et al., 2011). The CVDF comprises several scattered, small-volume andesitic and dacitic lava domes with high-K calc-alkaline and shoshonitic affinity formed intermittently between ca. 1 Ma and 0.3 Ma (Old Ciomadul eruptive period; OCEP) followed by the development of the more voluminous, dacitic Ciomadul volcanic complex (CVC) at ca. 160–30 ka (Young Ciomadul eruptive period; YCEP; Moriya et al., 1995, 1996; Vinkler et al., 2007; Harangi et al., 2010, 2015a, 2020; Molnár et al., 2018, 2019; Lahitte et al., 2019). The CVC is composed of amalgamated lava domes truncated by two deep explosion craters (Fig. 1; Karátson et al., 2013, 2016; Szakács et al., 2015). Pyroclastic deposits are confined only to the youngest, more explosive phase of
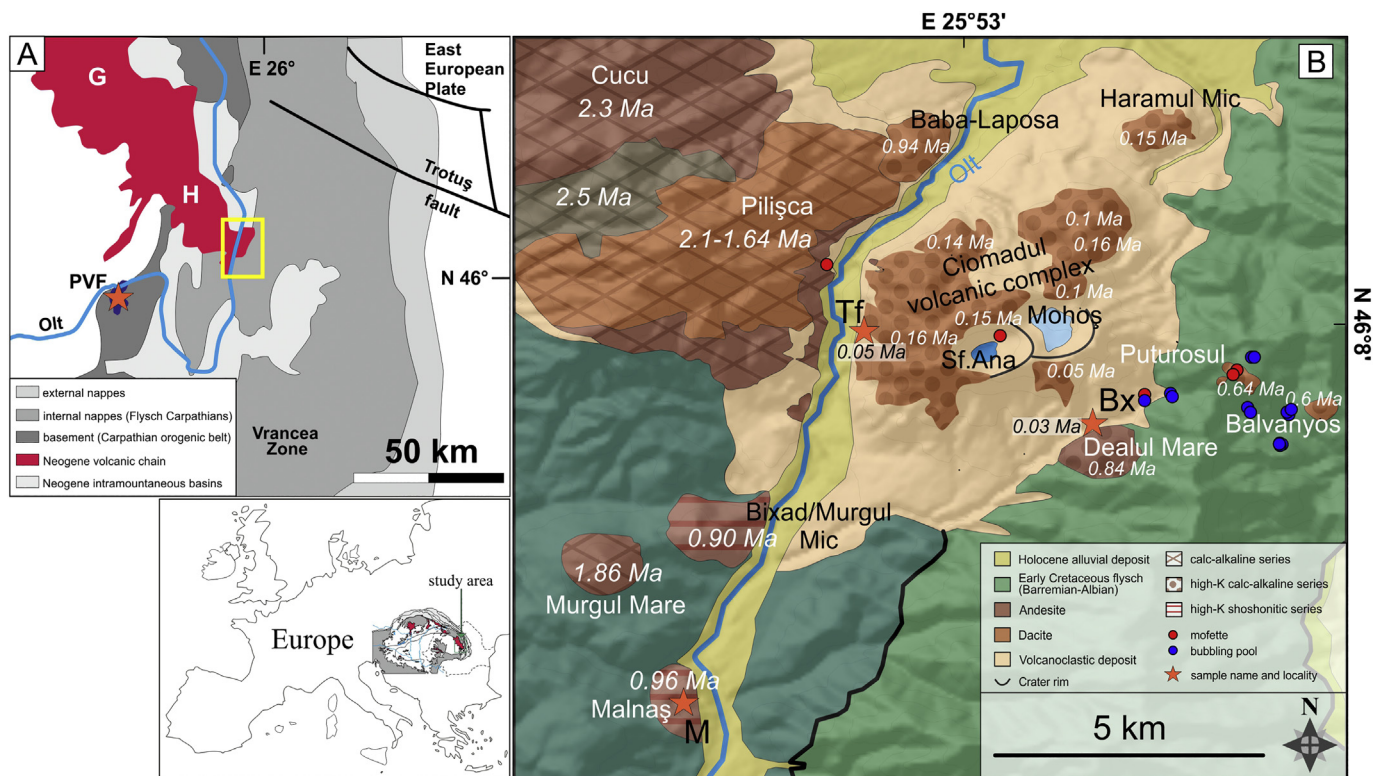

Fig. 1. Simplified tectonic map of the Călimani-Gurghiu Harghita volcanic chain (A) and a geological map of the studied area (B; yellow rectangle on map A; after Martin et al., 2006; Szakács et al., 2015 and Molnár et al., 2018). Sampling locations for the mofettes and bubbling pools are from Kis et al. (2019). Eruption ages in italic from Harangi et al., 2010, 2015a, Molnár et al., 2018, 2019. G: Gurghiu; H: Harghita; PVF: Perşani Volcanic Field; Bx: Bixad outcrop; Tf: Tuşnad outcrop, M: Malnaş quarry. (For interpretation of the references to color in this figure legend, the reader is referred to the web version of this article.)

activity at ca. 56–30 ka (Harangi et al., 2010, 2015a, 2020; Karátson et al., 2016; Molnár et al., 2019; Moriya et al., 1995, 1996; Vinkler et al., 2007), when several collapse events of the extruded lava domes were accompanied by Vulcanian and sub-Plinian eruptions.

The eruptive products of the YCEP (i.e., both lava domes and pyroclastics) are relatively homogeneous high-K calc-alkaline dacites (Molnár et al., 2018, 2019; Szakács et al., 1993; Szakács and Seghedi, 1987; Vinkler et al., 2007). The dacites are crystal-rich having a typical phenocryst assemblage of plagioclase, amphibole and biotite, whereas the shoshonites have low phenocryst content mostly consisting of clinopyroxene with amphibole and biotite in minor amount. Petrological studies revealed distinct amphibole populations and the existence of a long-lived (at least ca. 350 ky), low-temperature (~700–750 °C) crystal mush body at ~8–12 km depth, which was periodically remobilized by injection of hot, mafic magmas which triggered the volcanic eruptions (Harangi et al., 2015a, 2015b; Kiss et al., 2014; Laumonier et al., 2019). The presence of a melt-bearing magma body beneath the volcano at ~5–20 km depth and possibly at the lowermost crust (at ~30–40 km) was inferred by low electric resistivity anomalies (Harangi et al., 2015b) and low seismic velocity zones (Popa et al., 2012).

2.1. Present-day noble gas isotope systematics at Ciomadul

There is a large number of focused CO_2-rich degassing sites in the surroundings of Ciomadul volcano. They are mostly at the periphery of the CVC and are present as low-temperature (~8–10 °C) dry mofettes, bubbling pools and CO_2-bubbling peat bogs (Althaus et al., 2000; Jánosi et al., 2011; Kis et al., 2017, 2019; Vaselli et al., 2002) with a minimum of CO_2 flux of 8.7×10^3 t/y (Kis et al., 2017). The obtained R_c/R_A values (up to 4.5 R_A; Althaus et al., 2000; Vaselli et al., 2002; Kis et al., 2019; where R_c is the air-contamination corrected ${}^3He/{}^4He$ ratio of the sample and R_A is $(1.382 \pm 0.005) \times 10^{-6}$; Sano et al., 2013) indicate the presence of a mantle-derived component in the discharged gases. However, these values are lower than those recorded in olivine, orthopyroxene and clinopyroxene (6.1 ± 0.6 R_A) from the ultramafic xenoliths of PVF (Althaus et al., 1998; Faccini et al., 2020; Kis et al., 2019). Crustal contamination, magma aging and degassing (Althaus et al., 2000; Vaselli et al., 2002) can be accounted for the lower R_c/R_A values in the Ciomadul area, while Kis et al. (2019) suggested that the isotopic signature of the present-day emitted gases could reflect a strongly metasomatized lithospheric mantle beneath Ciomadul, which differs from the lithospheric mantle beneath Perşani. They proposed that the discharging gases did not originate from the shallow crustal magma storage but from a deeper zone (mantle-crust boundary), and the gases did not interact with the magma body at depth of 8–12 km during the upwelling.

3. Samples and analytical procedures

Two pyroclastic deposits and one lava dome of the CVDF were sampled together with a xenolith sample from La Gruiu scoria cone of the PVF (Fig. 1). To avoid the effect of possible cosmogenic ${}^3He$ addition (Marty et al., 1994), the samples were collected from deeper positions at the outcrops.

The two pyroclastic deposits crop out close to Bixad and Băile Tuşnad villages (hereafter Bx and Tf, respectively; Fig. 1), and represent the two most studied sites of the Ciomadul volcano (e.g. Harangi et al., 2010, 2015a, 2020; Karátson et al., 2016; Moriya et al., 1995, 1996; Vinkler et al., 2007). The Tf outcrop formed ca. 50 ka (Harangi et al., 2015a), whereas the eruption age obtained from the Bx outcrop is ca. 32 ka (Harangi et al., 2010, 2015a; Vinkler et al., 2007). The sampled pumiceous deposits belong to the youngest phase of activity of Ciomadul (ca. 56–32 ka; Eruptive Epoch 5; Harangi et al., 2015a; Molnár et al., 2019).

The small-volume shoshonitic lava dome close to the village of Malnaş represents the oldest eruptive product of the CVDF with an

eruption age of 964 ± 44 ka (Molnár et al., 2018). Here, unaltered, freshly-cut lava rock samples were collected from the quarry, where the mining activity dates back to the mid-19th century (Schafarzik, 1904).

Additionally, a peridotite xenolith was sampled from La Gruiu scoria cone of the nearby PVF (Fig. 1), to be used primarily as an in-house reference for the noble gas measurements, as the noble gas isotopic systematics of this area were already studied in detail (Althaus et al., 1998; Faccini et al., 2020; Kis et al., 2019).

The pumices and lava rock samples were crushed, sieved, and the 125–250 μm and 250–500 μm fractions were used for further separation. The plagioclase, amphibole and clinopyroxene fractions were concentrated with multi-step heavy liquid (sodium polytungstate) separation, magnetic separation and additional hand-picking under a binocular microscope.

The xenolith sample was crushed and sieved, then the 250–500 μm and 0.5–1 mm fractions were used for hand-picking the clinopyroxene and the orthopyroxene crystals under the binocular microscope.

The clinopyroxene, orthopyroxene, amphibole and plagioclase separates were ultrasonically cleaned in acetone before measurements.

0.25 to 1.75 g of each mineral phases were loaded into stainless-steel holders with a magnetic ball and baked at ~100 °C for 10–12 h in vacuum before the measurements. Gas was extracted from the mineral separates by single-step crushing (all mineral separates were crushed by 150 strokes, except for one clinopyroxene sample from the Perşani xenolith; Table 1) at room temperature (22 °C). The relatively low number of strokes was applied for each measurement in order to avoid significant contribution of an in-situ component. The analyses were performed at the Isotope Climatology and Environmental Research Centre, Institute for Nuclear Research, Debrecen (Hungary). Helium isotope abundances and ratios were determined by a HELIX- SFT mass spectrometer, whereas a VG-5400 mass spectrometer was used for neon and argon. The extracted gas was first collected in two steps in a duration of 40 min on two cryogenic traps cooled at 25 K (empty trap; for Ar) and 10 K (charcoal trap, for He and Ne). The trapped gases were then stepwise released from the charcoal trap at 42 K and 90 K for He and Ne measurements, respectively; and at 55 K from the empty trap for Ar measurement. The released He, Ne and Ar were purified by the built-in getters of the mass spectrometers. Ar was additionally purified by combined cold and hot getters (SAES, St 707). Known-volume air aliquots were repeatedly run through in the same way on the gas purification line for the calculation of concentrations. Concentrated calibration gases were measured on a daily basis to monitor and correct for the daily changes of the instruments. Signals were collected by a Faraday cup in the case of ${}^4He$ and ${}^{40}Ar$ and by an electron multiplier for all the other isotopes. Peak centering was manually done for the neon isotopes to avoid possible interferences from ${}^{40}Ar^{++}$ and ${}^{12}C^{16}O_2^{++}$ (e.g. Osawa, 2004), choosing the right plateau of the ${}^{40}Ar^{++}$-${}^{20}Ne$ and the left plateau of the ${}^{22}Ne$-${}^{12}C^{16}O_2^{++}$ double peaks although, the contribution of CO_2 molecule ions was negligible. The analytical procedures are described in more detail in Papp et al. (2012). Helium blanks averaged 1×10^{-11} ccSTP/g (ccSTP: cubic centimeter at standard temperature and pressure, 0 °C and 1 atm), neon blanks averaged 5×10^{-11} ccSTP/g, whereas argon blanks averaged 6×10^{-8} ccSTP/g. The analytical error of the measurements was <1% for ${}^4He$ and ${}^{40}Ar$, <5% for ${}^{20}Ne$, ${}^{22}Ne$ and ${}^{36}Ar$, and 3–10% for ${}^3He$ and ${}^{21}Ne$.

4. Results

4.1. General petrography of the pumices

A detailed study was reported by Vinkler et al. (2007) about the main petrographic and geochemical characteristics of the pumices of Ciomadul, which focused on the pre-eruptive processes. Here, we relied on their observations and some additional information was added being crucial for the data interpretation. The studied dacitic pumices from the

Table 1

Elemental and isotope composition of He-Ne-Ar in the measured mineral separates.

Volcanic district	Volcanic unit	Age	Sample	Rock type		Mineral	Weight (g)	number of strokes	He (ccSTP/g)	Ne (ccSTP/g)	Ar (ccSTP/g)	R/R_A	$^{20}Ne/^{22}Ne$	$^{21}Ne/^{22}Ne$	$^4He/^{20}Ne$	$^{40}Ar/^{36}Ar$	R_c/R_A	±	$^4He/^{40}Ar^*$
Ciomadul volcanic dome field	Eruptive Episode 5/1	55–45 ka	Tf	Dacite	Pumice	plag	1.3	150	4.9E−09	1.2E−09	7.8E−08	0.2	9.9	0.029	4.7	300.4	0.11	0.02	0.25
						plag	0.9	150	5.0E−09	8.1E−10	1.8E−07	0.1	9.9	0.031	6.7	330.6	0.07	0.02	0.13
						plag	1.7	150	1.8E−09	5.6E−10	1.1E−07	0.2	9.8	0.030	3.5	337.1	0.12	0.03	0.08
						plag	0.9	150	6.1E−09	5.3E−10	1.7E−07	0.1	9.6	0.028	12.6	514.0	0.06	0.01	
						amph	1.3	150	1.1E−08	3.4E−10	5.9E−08	0.4	9.6	0.029	34.7	302.9	0.39	0.08	
						amph	1.8	150	8.9E−09	1.8E−10	9.9E−08	0.5	9.9	0.029	55.5	308.7	0.53	0.08	
						amph	1.5	150	9.4E−09	1.9E−10	1.0E−07	0.8	9.2	0.028	54.2	506.2	0.77	0.17	0.22
	Eruptive Episode 5/2	34–30 ka	Bx	Dacite	Pumice	plag	1.7	150	3.0E−08	5.1E−09	2.0E−07	0.2	8.9	0.034	6.5	303.9	0.12	0.01	
						amph	1.8	150	4.1E−09	4.8E−09	1.9E−07	1.7	8.9	0.032	0.9	302.9	2.11	0.12	
						amph	1.2	150	1.7E−09	3.6E−09	8.2E−08	1.1	9.7	0.028	0.5	302.9	1.16	0.25	
	Eruptive Epoch 1	964 ± 46 ka	M	Trachyandesite	Lava rock	cpx	0.4	150	3.9E−09	5.9E−10	4.5E−07	3.2	10.0	0.029	7.3	311.4	3.25	0.66	0.17
						cpx	1.1	150	8.7E−10	1.7E−10	7.3E−08	3.7	10.0	0.031	5.8	300.3	3.81	0.85	
						cpx	1.0	150	1.8E−09	2.9E−10	9.2E−08	2.9	10.1	0.030	7.1	299.3	2.99	0.62	
						cpx	1.2	50	1.3E−09	1.5E−10	1.2E−07	2.1	10.4	0.031	9.7	304.2	2.13	0.52	
Perşani volcanic field		1.2–0.6 Ma		Peridotite	Xenolith	opx	1.5	150	3.8E−08	7.4E−11	1.2E−07	6.4	10.8	0.037	554.7	451.5	6.38	0.36	0.90
						cpx	0.3	150	1.3E−07	3.1E−10	7.8E−07	6.3	10.6	0.034	454.9	369.4	6.35	0.90	0.81
						cpx	1.3	50	4.1E−08	6.7E−11	1.9E−07	5.0	10.8	0.032	671.6	360.5	4.98	0.70	1.18
						cpx	1.3	100	5.4E−08	6.1E−11	2.1E−07	4.8	10.5	0.033	970.0	369.4	4.76	0.68	1.27

amph: amphibole, plag: plagioclase, opx: orthopyroxene, cpx: clinopyroxene, Tf: Tuşnad, Bx: Bixad, M: Malnaş.
$^4He/^{40}Ar^*$ were calculated only when $^{40}Ar/^{36}Ar$ > 310.

Bx and Tf outcrops display similar petrographic characteristics. These are high-K calc-alkaline dacites (SiO_2 = 65–68 wt%, K_2O = 3.1–3.3 wt%; Harangi et al., 2020). Their texture is porphyritic with a glassy groundmass and diverse vesicularity. The main phenocryst content is around 15–20 vol%, and is composed of (in the order of occurrence) plagioclase, amphibole and biotite (Fig. 2). The size of the plagioclase crystals varies between 0.2 and 4 mm, the smaller ones are always euhedral with usually clear texture, whereas the larger ones are subhedral or anhedral. The core of the larger plagioclase crystals and crystal clots for both localities (Tf and Bx) usually exhibit a sieved texture, with coexisting fluid and silicate melt inclusions, relics of amphibole and/or biotite and apatite needles. The edge of the plagioclase crystals is always clear from the Tf locality, whereas the resorbed edges with spongy or sieved texture are more characteristic for plagioclase from the Bx locality. The amphibole crystals are usually euhedral with normal, oscillatory or reverse zoning; their size varies between 0.5 and 1 mm. Some of the amphibole crystals have a resorbed core with the presence of ortho-, clinopyroxene and/or olivine in the case of the Bx locality (Vinkler et al., 2007). The accessory minerals are apatite, zircon and titanite.

Despite similarities in the phenocryst content, the pumices from the two outcrops show differences both in their whole-rock composition and in their plagioclase, amphibole (Fig. 3) and glass composition (Harangi et al., 2020; Vinkler et al., 2007). The Tf plagioclase covers wider range in more sodic composition ($An_{20–50}$), and the groundmass glass is more SiO_2-rich (~75–77 wt%) compared to the Bx plagioclase ($An_{40–60}$) and glass (SiO_2 = 70–75 wt%), respectively. The Tf amphibole phenocrysts are primarily low-Al type (Al_2O_3 < 9 wt%), whereas dominantly high-Al (Al_2O_3 > 10 wt%) amphibole phenocrysts are present at Bx locality (Fig. 3). These differences between the two localities (age, whole-rock, glass, mineral composition) make them a suitable target to detect how (or whether) the noble gas addition from the different reservoirs (air, crust, mantle) could have changed during the last 50 kyr.

4.2. General petrography of Malnaş shoshonite

General petrographic description of Malnaş shoshonite and its eruption age was given by Molnár et al. (2018), whereas Bracco Gartner et al. (2020) reported a detailed study on silicate melt inclusions in the phenocrysts. The studied sample is a trachyandesite with high-K calc-alkaline – shoshonitic affinity (SiO_2 = 57–58 wt%, K_2O = 3.5 wt%; Molnár et al., 2018). Its texture is porphyritic with a crystalline, coarse-grained groundmass, with a lower phenocrysts content (5–10%) compared to the pumices (Fig. 2). The dominant phenocrysts are primitive clinopyroxene (mainly diopside, mg#: 86–92 mol%; Fig. 4; Bracco Gartner et al., 2020) and altered feldspar; biotite, amphibole, orthopyroxene, olivine and rounded quartz can occur as minor constituents. The groundmass is mainly composed of clinopyroxene and feldspar, whereas the accessories are titanite, zircon and apatite.

4.3. Fluid- and silicate melt inclusion petrography

Large number of coexisting, primary fluid (FI) and silicate melt inclusions (SMI) were observed in plagioclase, amphibole and biotite host minerals from both locations in the studied samples (Fig. 2). The primary fluid inclusions had usually dark color and one phase at room temperature, but two-phase inclusions were also observed with dark color liquid and gas phase. Their size was below 10 μm with rounded or oval shape. The silicate melt inclusions had negative-crystal shape and contain glass and bubble(s) from the Tf locality, whereas from the Bx locality they were rounded or irregular, causing the spongy textures of the host mineral. The dark-colored bubble had one phase at room temperature, and the glass phase was colorless. The bubble-glass ratio was varying between 0 (no glass) and 80%. The edge of the inclusions seemed to be intact. The primary SMIs occurred either along growth zones or in scattered position within the host minerals (Fig. 2). Their size was 5–80 μm within the plagioclase, whereas they were smaller, 5–30 μm
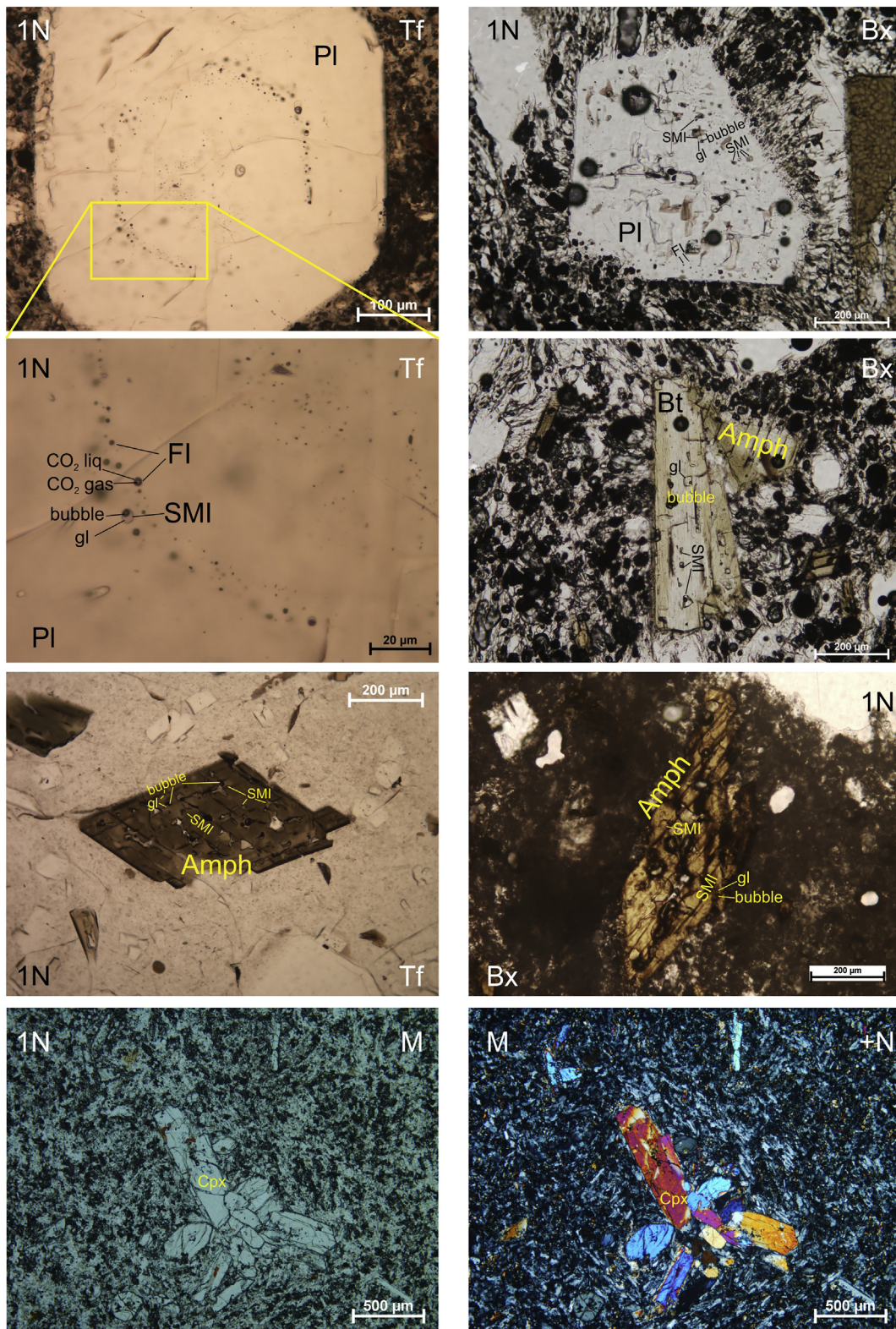
Fig. 2. Typical occurrences of the fluid inclusions hosted in amphibole and plagioclase from the two dacitic pumices and a general microscopic photo of the Malnaş shoshonite. Tf: Tuşnad locality; Bx: Bixad locality; M: Malnaş locality; Pl: plagioclase; Amph: amphibole; Bt: biotite; Cpx: clinopyroxene; FI: fluid inclusion; SMI: silicate melt inclusion; gl: glass; 1 N: plane polarized; +N: cross polarized.

in the mafic minerals. Silicate melt inclusions from Bx locality had similar habits in color, components and bubble-glass ratio, but their shapes were rounded, irregular and worm-like.

In the following, the term 'fluid inclusion' refers to the noble gas content extracted from the fluid inclusions and the bubble of the silicate melt inclusion. In the case of plagioclase, the <500 μm fraction was
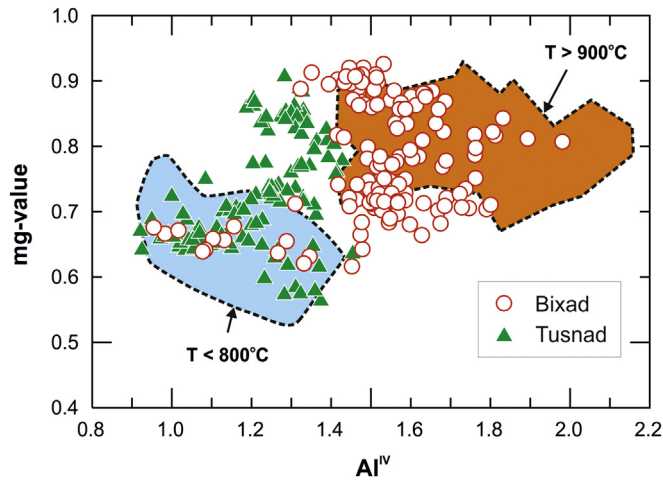
Fig. 3. Compositional features of the amphibole phenocrysts in the Bixad and Tuşnad dacitic pumices. Temperature values are based on experimental data compiled by Kiss et al. (2014). Note that the Tuşnad amphiboles are mostly low-Al type formed at low temperature, whereas the Bixad amphiboles are dominantly high-T crystals. Data are from Vinkler et al. (2007), Laumonier et al. (2019), Harangi et al. (2020) and unpublished data.
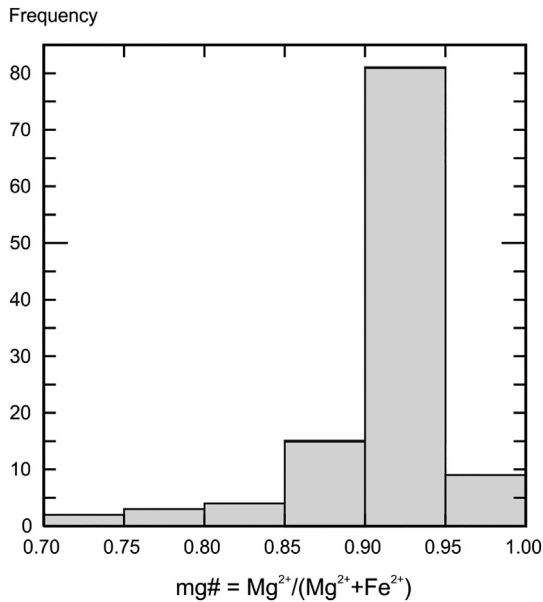

Fig. 4. Most of the clinopyroxenes in the Malnaş shoshonite have high mg-values suggesting crystallization from primitive magma. Data are from Bracco Gartner et al. (2020).

used, in order to reduce the possible amount of the larger grain-fragments with the strongly sieved texture.

4.4. Noble gas isotopic composition

We determined the He-Ne-Ar isotope composition of fluid inclusions hosted in plagioclase, amphibole, clinopyroxene and orthopyroxene, the results are presented in Table 1, Fig. 5 and the Supplementary file.

The noble gas concentrations of plagioclase and amphibole from the pumices, and of clinopyroxene from the Malnaş shoshonite were generally low, sometimes at or even below the instrumental detection limit, the latter being excluded from further interpretation. Helium concentrations varied between 1.7×10^{-9} and 3×10^{-8} ccSTP/g for the

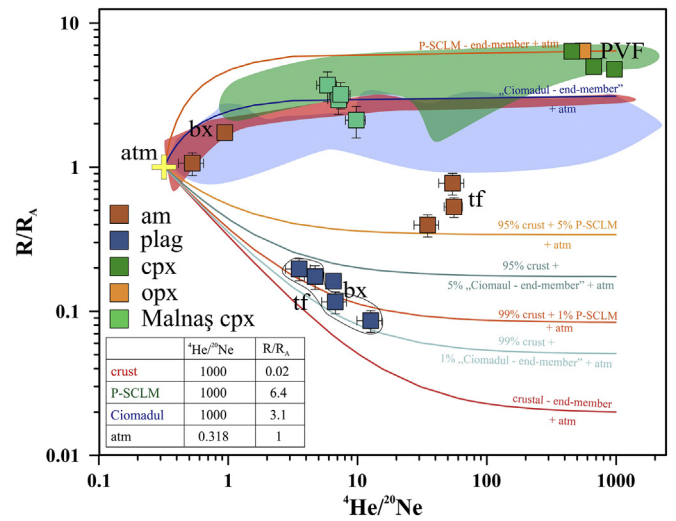**Fig. 5.** Helium isotopic ratios (R/R_A) and $^4He/^{20}Ne$ relationships with their uncertainties (equivalent with the size of the rectangle unless marked otherwise) of the studied mineral phases in comparison with the present-day gas composition (Kis et al., 2019). Blue and red areas represent the isotopic compositions of the bubbling pools and mofettes, respectively; whereas the green field indicates the isotopic composition of pyroxenes from the PVF (Althaus et al., 1998; Faccini et al., 2020; Kis et al., 2019). The assumed end members for He-isotopic ratios and $^4He/^{20}Ne$ ratios are: atmospheric (atm; 1 R_A, $^4He/^{20}Ne = 0.318$, Sano and Wakita, 1985); Perşani-Subcontinental Lithospheric Mantle (P-SCLM; 6.4 ± 0.4 R_A and $^4He/^{20}Ne$ ratio = 1000; this study). The typical crustal end-member is 0.02 R_A and $^4He/^{20}Ne$ ratio = 1000 (Sano and Marty, 1995), whereas a possible Ciomadul end-member: 3.1 ± 0.1 R_A and $^4He/^{20}Ne$ ratio = 1000 (Kis et al., 2019). The colored lines indicate binary (P-SCLM + atm, Ciomadul + atm and crust + atm) and ternary mixing trends of atmospheric helium with mantle-originated and crustal helium (Pik and Marty, 2009). (For interpretation of the references to color in this figure legend, the reader is referred to the web version of this article.)

Ciomadul pumices, while those from the shoshonite and xenolith samples were 8.7×10^{-10} to 3.9×10^{-9} ccSTP/g and 3.8×10^{-8} to 1.3×10^{-7} ccSTP/g, respectively. The $^3He/^4He$ values were corrected for the atmospheric contamination based on the measured $^4He/^{20}Ne$ ratios (Sano and Wakita, 1985). The R_c/R_A ratio of the mineral phases from Ciomadul pumices varied between 0.06 and 2.11 R_A, whereas those of the Malnaş clinopyroxene varied from 2.13 to 3.81 R_A (Fig. 5). The ortho- and clinopyroxene from the peridotite xenolith ranged between 4.76 and 6.37 R_A overlapping with the previously reported R_c/R_A ratios for the PVF (2.3–9.5 R_A; Althaus et al., 1998; Kis et al., 2019; Faccini et al., 2020; Fig. 5). The plagioclase R_c/R_A ratios from the Ciomadul pumices were rather uniform, varying between 0.06 and 0.12 R_A, whereas amphibole R_c/R_A ratios showed some differences between the two outcrops, being 0.39–0.77 R_c/R_A and 1.15–2.11 R_c/R_A for Tf and Bx, respectively (Fig. 5). The uncertainties of the He concentrations varied between 2 and 18%. The usually low He/noble gas content in these fluid inclusions, especially in the plagioclase separates accounts for the higher uncertainties.

The Ne content ranged between 1.8×10^{-10} and 5.1×10^{-9} ccSTP/g for the Ciomadul pumices, 1.5×10^{-10}-5.9×10^{-10} ccSTP/g for the Malnaş shoshonite, and between 6.1×10^{-11} and 3.1×10^{-10} ccSTP/g for the xenoliths. The $^{20}Ne/^{22}Ne$ ratios varied between 8.9 and 10.8, whereas the $^{21}Ne/^{22}Ne$ ratios ranged between 0.028 and 0.037 (Table 1). The $^4He/^{20}Ne$ ratios were in the range between 0.5 and 970 (Fig. 5). Although some samples showed slightly different isotopic composition than that of the air, indicating the presence of nucleogenic and mantle Ne components, due to the relatively large uncertainties (4–14%) and air contamination these values were not discussed in detail. The $^{40}Ar/^{36}Ar$ ratios were between 299 and 514 for the Ciomadul samples, whereas the xenoliths showed values just slightly higher than that of the air (295.5), between 360 and 451. The $^4He/^{40}Ar*$ ratios

were calculated for samples having $^{40}Ar/^{36}Ar > 310$ ($^{40}Ar^*$ represents the air contamination corrected ^{40}Ar). The Ciomadul separates had a range of 0.1–0.2, whereas the Perşani xenoliths varied between 0.8 and 1.3. Since the majority of the argon values, similarly to neon values, showed air contamination, they were not discussed further in details in the following sections.

5. Discussion

Noble gases are very sensitive geochemical tracers for identifying the source of a fluid (i.e., air-, crust- or mantle-derived; Hilton et al., 2002). The isotopic signature of helium (and neon) is an especially widely-used tool in subduction zone-related studies, whereas the application of neon and argon isotope systematics is more restricted due to the frequent case of air contamination (e.g., Hilton et al., 2002; Kis et al., 2019; Martelli et al., 2004; Rizzo et al., 2015, 2016; Sano and Wakita, 1985).

The noble gas systematics for present-day active arc-related volcanism cover a wide range of R_c/R_A values from 0.01 to 8.9 R_A, with a mean value of 5.37 ± 1.87 R_A (Hilton et al., 2002 and references therein). The highest reported values fall within the range of the MORB values (8 ± 1 R_A; Graham, 2002) implying a dominant contribution of mantle-derived helium. The lower $^{3}He/^{4}He$ ratios (<8 R_A) can be related to two-component mixing between mantle-derived and radiogenic helium. The rate of mixing is strongly affected by the contribution of radiogenic helium, which can depend on i) type of subduction (e.g. Hilton et al., 1992) ii) rate of mantle metasomatism (e.g. Martelli et al., 2004) iii) shallow crustal contamination (e.g. Sano et al., 1989) iv) near-surface magmatic degassing (e.g. Hilton et al., 2002) and v) magma aging (e.g. Martelli et al., 2004).

5.1. Helium and neon isotopic composition of the youngest eruption products

We analyzed the He, Ne and Ar isotopic composition of five plagioclase- and five amphibole separates in total, from a pyroclastic flow deposit (Bx) and a pyroclastic fall deposit (Tf), which are related to the ca. 32 ka and 50 ka explosive eruptions of the CVC, respectively (Table 1, Harangi et al., 2015a). Three groups can be defined according to their R/R_A and $^{4}He/^{20}Ne$ ratios (Fig. 5). The first group includes plagioclase from both Bx and Tf localities. Their R/R_A and $^{4}He/^{20}Ne$ ratios are quite uniform, between 0.09 and 0.19 and 3.5–12.5, respectively. Besides the small amount of atmosphere-originated fluids, these separates carry a clear crustal (radiogenic) signature (Fig. 5). The atmospheric component can be explained by either pre-eruptive, near-surface degassing (e.g. Hilton et al., 2002) or post-eruptive entrapment of air (e.g. Nuccio et al., 2008). The second group is represented by the Tf amphibole phenocrysts, their R/R_A ratios vary between 0.40 and 0.77, whereas the $^{4}He/^{20}Ne$ ratios show a lower amount of atmosphere-originated fluids compared to the plagioclase (Fig. 5). The third group refers to the Bx amphibole phenocrysts, where the highest R/R_A values (1.06–1.73) are recorded although characterized also by the strongest atmospheric contamination (0.5–0.9 $^{4}He/^{20}Ne$, Fig. 5). This is the only group from the pumices samples, where the compositions overlap with some of the measured $^{3}He/^{4}He$ ratios from the present-day CO_2-emission (Fig. 5; Kis et al., 2019) indicating the presence of a mantle component. The Bx amphiboles, generally pargasite with >10 wt% Al_2O_3, have distinct mineral chemistry compared to the Tf amphiboles (Fig. 3; Vinkler et al., 2007; Harangi et al., 2020), which are hornblende with <10 wt% Al_2O_3 and characterized by lower, more radiogenic $^{3}He/^{4}He$ isotope ratios. Petrological studies revealed that the high-Al amphiboles formed at higher temperature (>850 °C) reflecting probably the presence and effect of fresh, hot magma batch in the magma storage system (Kiss et al., 2014; Vinkler et al., 2007), also supported by the >1 R/R_A values. On the other hand, the low-Al amphiboles, together with the plagioclase phenocrysts represent a low-temperature

(700–750 °C) crystal mush assemblage which existed for a protracted time (>100 kyr) in the magma reservoir before the eruption (e.g. Harangi et al., 2015a; Kiss et al., 2014).

The lack of a clear mantle signature for most phenocryst separates is not an unusual phenomenon for subduction-related systems (e.g. Graham et al., 1993; Hilton et al., 1992, 1993, 2002; Martelli et al., 2004) and the lower R/R_A values at Ciomadul can be related to several distinct processes: i) magma aging of a long-lived magma storage can lower the $^{3}He/^{4}He$ ratios by the production of ^{4}He from the U-Th decay chain ii) assimilation of the surrounding country rocks (e.g. Cretaceous flysch sediments; Ianovici and Rădulescu, 1966) characterized by lower $^{3}He/^{4}He$ ratio, which is admixed to the original magma iii) preferential ^{3}He loss relative to ^{4}He by diffusion and iv) contribution of in-situ ^{4}He ingrowth from the U and Th decay. Amphibole and plagioclase can contain zircon and apatite crystals as inclusions, which could contribute to the in-situ radiogenic ^{4}He amount from the U and Th decay (e.g. Farley, 2002). However, the gentle crushing applied to the samples allows to exclude this contribution. $^{4}He/^{40}Ar^*$ ratios can be used to trace the diffusive fractionation effects. However, most Ar measurements yielded air-like noble gas compositions and consequently, this cannot be easily and unambiguously constrained. The obtained $^{4}He/^{40}Ar^*$ values calculated for the separates with $^{40}Ar/^{36}Ar > 310$ vary between 0.08 and 0.25 (Table 1) indicating that these might be influenced by helium loss as these values are lower than the assumed production ratio for the mantle (1.6–4.2; Graham, 2002). Although the lack of robustness of the dataset does not make it possible to exclude completely the possibility of diffusive fractionation, the primitive clinopyroxene separate from the Malnaş shoshonite exhibits similarly low $^{4}He/^{40}Ar^*$ ratio (0.17; Table 1). This suggests that the ratios observed in plagioclase and amphibole cannot solely be explained by this process. The other two processes (the role of magma aging and crustal assimilation), which can explain the lower R/R_A values, are discussed in detail in the following sections.

5.2. Tracing the noble gas signature of the lithospheric mantle beneath Ciomadul

In order to evaluate the possible effect of magma aging, it is necessary to constrain the pristine noble gas composition of the source magma. The Malnaş shoshonite represents one of the least evolved eruption products of the CVDF and marks the onset of Ciomadul volcanism at ca. 1 Ma (Molnár et al., 2018). Clinopyroxene phenocrysts are mainly diopside with relatively high Mg# (86–92 mol%; Bracco Gartner et al., 2020). The mafic K-alkaline melts can be derived from a lithospheric mantle source affected by melt- and fluid-metasomatization (Bracco Gartner et al., 2020), which could be a possible source region of more mafic magmas during Ciomadul volcanism. Three clinopyroxene separates show quite uniform R/R_A and $^{4}He/^{20}Ne$ ratios of 2.9–3.7 and 5.3–7.3, respectively, while the fourth one has a slightly lower R/R_A ratio of 2.1, likely related to analytical uncertainty, since this exhibits the lowest ^{3}He content close to the detection limit. These values (3.2 ± 0.4 R_A) are lower than the average Perşani R/R_A values (6.1 ± 0.6 R_A; Althaus et al., 1998; Kis et al., 2019; Faccini et al., 2020), also confirmed by our analyses (6.3–6.4 R_A and 455–555 $^{4}He/^{20}Ne$ ratios; Fig. 5; Table 1).

Clinopyroxene phenocrysts and olivine-hosted silicate melt inclusion data from the Malnaş shoshonite (Bracco Gartner et al., 2020) revealed that the mafic K-alkaline melts are likely to be originated from a strongly metasomatized lithospheric mantle, which differs from the lithospheric mantle sampled by the Perşani alkaline basaltic melts. Thus, the measured R/R_A values of Malnaş clinopyroxene likely reflect the original noble gas signature of the lithospheric mantle, which is distinct by the degree of mantle metasomatism from the lithospheric mantle represented by the Perşani xenoliths.

Therefore, the helium isotopic composition of the clinopyroxene can be considered as the original, highly metasomatized noble gas signature

of the lithospheric mantle beneath the Ciomadul volcanic dome field. This is also supported by the present-day gas emission measurements, which revealed a similar possible end-member for lithospheric mantle noble gas composition of 3.1 ± 0.1 R$_A$ (Kis et al., 2019).

5.3. The effect of the long-lived magmatic system on the He composition

The possible magma-aging effect can lower the original R$_c$/R$_A$ value by adding radiogenic ^{4}He into the system via the decay of U and Th (e.g. Ballentine and Burnard, 2002) within the magma storage system. The apparent negative correlation between the measured ^{4}He contents and the R$_c$/R$_A$ ratios in the high-Al and low-Al amphiboles indicates the possibility of ^{4}He addition (Fig. 6). Harangi et al. (2015a) showed that the lifetime of the Ciomadul volcanic complex can be at least 350 kyr based on zircon U-Th crystallization ages and that the most intense zircon crystallization took place at ca. 140–130 ka. Therefore, the original noble gas composition can be modified during the long lifetime of the crystal mush. With a known starting composition and whole-rock U and Th content, the addition of the radiogenic ^{4}He, i.e. the decrease of the R/R$_A$ values can be computed (equations from Ballentine and Burnard, 2002):

^{4}He (atoms/g*yr) $= 3.24 \times 10^6$[U] $+ 7.710 \times 10^5$[Th]
^{3}He (atoms/g*yr) $= 1.68 \times 10^{-2}\{0.01$[U] $\times (13.8$[Na] $+ 5.4$[Mg] $+ 5$ [Al] $+ 1.31$[Si] $+ 2$[C]) $+ 0.01$[Th] $\times (6.0$[Na] $+ 2.45$[Mg] $+ 2.55$[Al] $+ 0.56$[Si] $+ 0.83$[C]) $+ 0.4788$[U]\}$

We computed the evolution of the R/R$_A$ ratio of a possible mantle-originated fluid (Fig. 7) by using the whole-rock composition of Bx and Tf samples (Vinkler et al., 2007) with an initial ^{4}He and ^{3}He concentrations of an orthopyroxene and a clinopyroxene from PVF measured in this study and the Malnaş clinopyroxene with the highest He concentration. The calculations for the different scenarios are presented in the Supplementary Material, whereas the most plausible scenarios are shown in Fig. 7 and Table 2.

With a starting composition measured from the PVF orthopyroxene (^{3}He: 3.32×10^{-13} ccSTP/g and ^{4}He: 3.76×10^{-8} ccSTP/g), the decrease of the R/R$_A$ values is significant (Fig. 7). After 150 kyr of residence time, from 6.4 R$_A$ a value of 1.4 R$_A$ is achieved. This is mainly due to the low initial concentrations of He and the relatively high whole-rock U and Th concentrations. The PVF clinopyroxene has larger amount of He (^{3}He: 1.11×10^{-12} ccSTP/g and ^{4}He: 1.27×10^{-7} ccSTP/g) therefore, the decrease is less dramatic. After 150 kyr of residence time, the initial R$_A$ value of 6.4 drops down to 3.1 (Fig. 7). The R/R$_A$ decrease computed based on the orthopyroxene-hosted fluid inclusion seems to be unrealistic, the R$_A$-decrease from the clinopyroxene-hosted fluid inclusion was
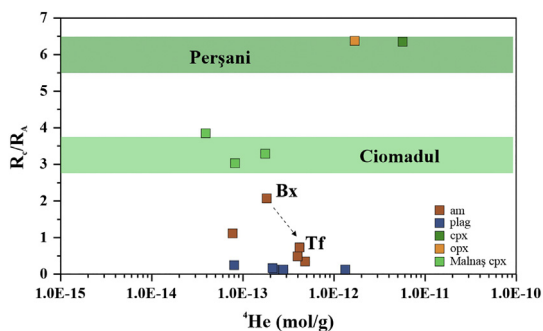
Fig. 7. The evolution of R/R$_A$ values through time with the different starting He isotopic compositions and whole rock geochemistry data. The R/R$_A$ values at 50, 100 and 150 kyr residence times are marked.

applied to trace the mantle contribution. Regardless of the initial compositions, the decreased values by magma aging are still higher than the measured R/R$_A$ in the amphibole and plagioclase from Bx and Tf localities, and cannot explain solely the observed ratios.

In the case of starting compositions of the Malnaş clinopyroxene separate with the highest He concentration (^{3}He: 1.72×10^{-14} ccSTP/g and ^{4}He: 3.94×10^{-9} ccSTP/g), the decrease in the R/R$_A$ values is quite pronounced, from a starting 3.2 R$_A$ value it can reach as low as 0.1 R$_A$ during 150 kyr of residence time (Fig. 7). However, due to at least one order of magnitude lower concentrations than the Perşani separates, this decrease in the R$_A$ values can be slightly overestimated.

The decreased values are covering the range of the measured R/R$_A$ values in the case of the Bx and Tf amphibole with the Malnaş initial composition, and considering low He concentrations. This is supported by the similar low amounts measured in amphibole and plagioclase from both localities. For the Bx amphibole, the measured noble gas composition can be explained by even <10 kyr of residence time, whereas in the case of the Tf amphiboles ca. 20–50 kyr of residence time is required if solely the magma aging is considered as the modifying effect.

The measured R/R$_A$ values of the plagioclase separates can be explained by the effect of magma aging only if the Malnaş initial composition with a prolonged residence time of 100–150 kyr is taken into account. Considering the much shorter residence time in the case of amphibole, it does not seem realistic that this was the only modifying factor in the noble gas composition. The lower ratios would imply likely a certain amount of crustal fluid contribution or the magma was affected by partial degassing and lost part of its noble gas content.

5.4. Three-component mixing

Assuming crustal fluid contribution to the noble gas compositions of the trapped fluids, three noble gas components can be considered: i) mantle ii) air and iii) crust. To evaluate the contribution of these sources, the isotopic composition of these possible end-members is to be defined: atmosphere (atm): 1 R$_A$, ^{4}He/^{20}Ne $= 0.318$ (Sano and Wakita, 1985), crust: 0.02 R$_A$ and ^{4}He/^{20}Ne $= 1000$ (Sano and Marty, 1995). More questionable are the values for the mantle end-member.

Fig. 6. The relation of the measured ^{4}He contents and R$_c$/R$_A$ ratios of the separates. The green field represent the possible lithospheric end-members beneath the region: Perşani end-member: 6.1 ± 0.6 R$_A$ (Althaus et al., 1998; Kis et al., 2019; Faccini et al., 2020; this study), Ciomadul end-member: 3.2 ± 0.4 R$_A$ (Kis et al., 2019; this study). am: amphibole, plag: plagioclase; cpx: clinopyroxene, opx: orthopyroxene. (For interpretation of the references to color in this figure legend, the reader is referred to the web version of this article.)
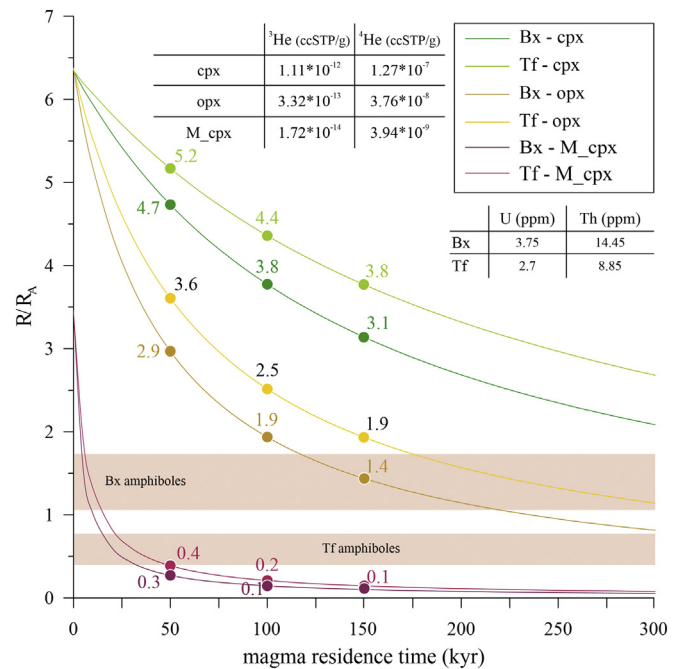
Table 2

Changes in the R/R$_A$ values based on different U and Th content and initial He concentrations through magmatic residence time. The bold values are used for the three-component mixing calculations.

Sample	Initial concentrations		Residence time	Bx whole-rock (U 2.7, Th 8.9 ppm[*])					Tf whole-rock (U 3.8, Th 14.5 ppm[*])				
	^{3}He	^{4}He		0 kyr	5 kyr	50 kyr	100 kyr	150 kyr	0 kyr	5 kyr	50 kyr	100 kyr	150 kyr
opx (PVF)	3.32*10^{-13}	3.76*10^{-8}	**R/R$_A$**	6.4	5.7	3.0	1.9	1.4	6.4	5.9	3.6	2.5	1.9
cpx (PVF)	**1.11*10^{-12}**	**1.27*10^{-7}**		**6.3**	6.1	4.7	3.8	3.1	**6.3**	6.2	5.2	4.4	3.8
Malnas_cpx	**1.72*10^{-14}**	**3.94*10^{-9}**		**3.2**	**1.5**	0.3	0.1	0.1	**3.2**	**1.8**	0.4	0.2	0.1

[*] Data from Harangi et al. (2020).
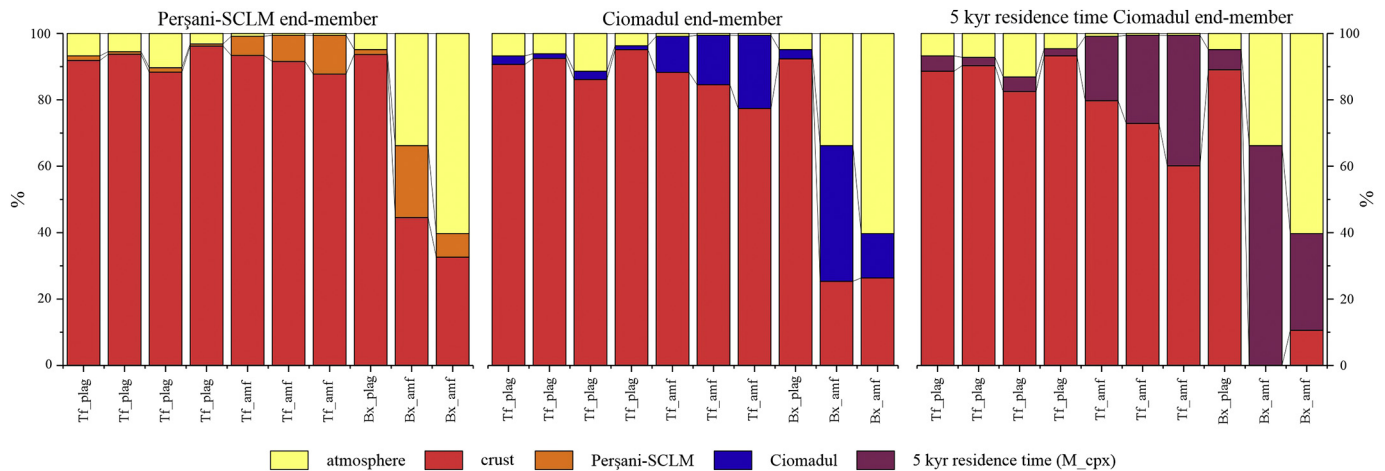
Fig. 8. Three-component mixing calculations with the possible mantle end-members. Mantle-, crustal- and atmospheric fluid contributions (%) for the Perşani-Subcontinental Lithospheric end-member (left panel); the metasomatized 'Ciomadul' mantle end-member (middle panel) and in the case of a 5 kyr of residence time with the 'Ciomadul' initial composition (right panel).

One possibility is to use the subcontinental lithospheric mantle composition of the PVF (P-SCLM; 6.4 ± 0.4 R$_A$ and ^{4}He/^{20}Ne = 1000; Fig. 5). However, Kis et al. (2019) suggested that the mantle beneath Ciomadul is likely to have a lower value of 3.1 ± 0.1 R$_A$. This is comparable with the noble gas signature of the Malnaş clinopyroxene with a R/R$_A$ ratio of 3.2 ± 0.4 (with ^{4}He/^{20}Ne = 1000; hereafter 'Ciomadul' end-member) for a mantle source that was largely modified by metasomatism. For the three-component mixing calculation we used these possible mantle end-member values (P-SCLM and 'Ciomadul'), together with two mantle-end members affected by the magma aging (5 kyr and aged 'Ciomadul'; Table 2). The results of the three-component mixing calculations with different mantle end-member values are presented in Fig. 8.

In the case of plagioclase, regardless of the sample locality and different mantle end-member values, the contribution of crustal fluids is dominant (>90%, Fig. 8). For the Bx high-Al amphibole, the mantle contribution is at least 22% using the P-SCLM end-member, while with the 'Ciomadul' end-member it reaches 41%. If we consider a few kyr's of magma aging, its composition can solely be explained by a two-component mixture of 'Ciomadul' mantle and air. Therefore, at least a ~ 50–60% of mantle fluid contribution during the crystallization of amphibole before the last eruptive episode of Ciomadul might be regarded as reliable. In the case of the Tf low-Al amphibole, regardless of the proposed end-members, the mantle contribution is relatively low: 12% and 22% for the P-SCLM and 'Ciomadul' end-members, respectively (Fig. 8). Assuming few kyr's of magma aging with the 'Ciomadul' initial end-member, the mantle contribution reaches 39% (Fig. 8), whereas in the case of ca. 30 kyr of residence time and the 'Ciomadul' initial composition, the measured R/R$_A$ ratios can be explained (Fig. 7) as a mixture of mantle fluids and minor air contribution. However, the addition of small amount of crustal fluids cannot be excluded with such a

prolonged residence time. Therefore, a maximum of ~20–30% of mantle fluid contribution can be estimated during the crystallization of the amphibole, before the explosive eruptions at ca. 50 ka.

The difference in the noble gas compositions (and the proposed mantle fluid contributions) for the Bx and Tf amphibole is also supported by the different geochemical composition (Harangi et al., 2020; Laumonier et al., 2019; Vinkler et al., 2007), with Bx showing a higher temperature, fresh magma contribution and higher mantle-fluid contribution. The strong crustal-fluid contribution for plagioclase from both locations (despite their differences in their geochemical composition; Vinkler et al., 2007) is consistent with its slightly later-stage crystallization compared to that of amphibole where only crustal fluids are present. Based on Sr-Nd-O isotopic compositions, small-scale assimilation of flysch sediments in upper-crustal levels and the presence of an already enriched source were assumed (Mason et al., 1996). However, it should be noted that ~1% (or less) country-rock assimilation/interaction can be responsible for <1 R/R$_A$ values without affecting the isotopic compositions (Hilton et al., 1993), and this can explain the measured noble gas compositions in the phenocrysts.

6. Conclusion

In this study, we analyzed the noble gas isotopic composition of fluid inclusions in amphibole and plagioclase phenocrysts from two explosive products of the Ciomadul volcanic complex; and clinopyroxene phenocrysts from the oldest, least evolved lava dome of Ciomadul volcanic dome field. The high-mg Malnaş clinopyroxene exhibits the highest R$_c$/R$_A$ values (3.2 ± 0.4 R$_A$), which is in the range of the end-member value defined by the present-day gas emissions (Kis et al., 2019). The R$_c$/R$_A$ values of the high-Al amphibole (1.16–2.11 R$_A$) from Bixad locality also overlap with the noble gas signature of the present-day CO$_2$

emissions. This sample shows the highest proportion (at least 60%) of mantle fluid contribution, which is the result of a fresh magma recharge event and shorter residence time before the eruption. The low-Al amphibole from Tuşnad locality exhibits lower R_c/R_A values (0.39–0.77 R_A), and shows a lower amount (~20–30%) of mantle-fluid contribution. The plagioclase from both localities are defined by a dominant crustal origin having R_c/R_A values of 0.06–0.12. The low-Al amphibole and the plagioclase phenocrysts represent a low-temperature crystal mush assemblage with protracted residence time in the magma reservoir, thus their primary noble gas signature could be modified by magma aging, contribution of crustal fluid and/or diffusive fractionation. The lack of larger proportion of >1 R_c/R_A values in the youngest eruption products supports the suggestion of Kis et al. (2019) that the mantle fluids of the present-day emissions did not or just partly touched the Ciomadul magma storage system, or degassed at lower depth.

The newly-measured noble gas compositions from peridotite xenoliths from the Perşani Volcanic Field (6.4 ± 0.4 R_A) are in agreement with the previously reported values (Althaus et al., 1998; Faccini et al., 2020; Kis et al., 2019), but differ significantly from those measured in mofettes in the Ciomadul area (Kis et al., 2019) and from the maximum values measured both in the high-Al amphibole (2.11 ± 0.1 R_A) and clinopyroxene phenocryst of Malnaş (3.7 ± 0.8 R_A) in this study.

The new results strengthen previous findings that the primitive Ciomadul magmas can be characterized by a relatively low R/R_A signature as a result of intense mantle metasomatism and reinforce the conclusions about the different rate of mantle metasomatism and small-scale heterogeneities of the lithospheric mantle beneath the region.

Declaration of Competing Interest

None.

Acknowledgements

Appendix A. Supplementary data

Supplementary data to this article can be found online at https://doi.org/10.1016/j.lithos.2021.106152.

References

Althaus, T., Niedermann, S., Erzinger, J., 1998. Noble gases in ultramafic mantle xenoliths of the Persani Mountains, Transylvanian Basin, Romania. Mineral. Mag. 62A (1), 43–44. https://doi.org/10.1180/minmag.1998.62A.1.23.

Althaus, T., Niedermann, S., Erzinger, J., 2000. Noble gas studies of fluids and gas exhalations in the East Carpathians, Romania. Chem. Erde 60, 189–207.

Ballentine, C.J., Burnard, P.G., 2002. Production, release and transport of noble gases in the continental crust. Rev. Mineral. Geochem. 47 (1), 481–538. https://doi.org/10.2138/rmg.2002.47.12.

Battaglia, A., Bitetto, M., Aiuppa, A., Rizzo, A.L., Chigna, G., Watson, I.M., D'Aleo, R., Juárez Cacao, F.J., de Moor, M.J., 2018. The magmatic gas signature of Pacaya volcano, with implications for the volcanic CO2 flux from Guatemala. Geochem. Geophys. Geosyst. 19 (3), 667–692. https://doi.org/10.1002/2017GC007238.

Bracco Gartner, A.J.J., Seghedi, I., Nikogosian, I.K., Mason, P.R.D., 2020. Asthenosphere-induced melting of diverse source regions for East Carpathian post-collisional volcanism. Contrib. Mineral. Petrol. 175, 54. https://doi.org/10.1007/s00410-020-01690-4.

Caracausi, A., Favara, R., Giammanco, S., Italiano, F., Paonita, A., Pecoraino, G., Rizzo, A., 2003. Mount Etna: Geochemical signals of magma ascent and unusually extensive plumbing system. Geophys. Res. Lett. 30 (2), 1057. https://doi.org/10.1029/2002GL015463.

Caracausi, A., Martelli, M., Nuccio, P.M., Paternoster, M., Stuart, F.M., 2013. Active degassing of mantle-derived fluid: a geochemical study along the Vulture line, southern Apennines (Italy). J. Volcanol. Geotherm. Res. 253, 65–74. https://doi.org/10.1016/j.jvolgeores.2012.12.005.

Correale, A., Pelorosso, B., Rizzo, A.L., Coltorti, M., Italiano, F., Bonadiman, C., Giacomoni, P.P., 2019. The nature of the West Antarctic Rift System as revealed by noble gases in mantle minerals. Chem. Geol. 524, 104–118. https://doi.org/10.1016/j.chemgeo.2019.06.020.

Jánosi, Cs, Berszán, J., Péter, É., 2011. The mineral baths of Ciomadul Mountains. Acta Siculica 2011, 41–56 Miercurea Ciuc. (In Hungarian).

Daskalopoulou, K., Gagliano, A.L., Calabrese, S., Longo, M., Hantzis, K., Kyriakopoulos, K., D'Alessandro, W., 2018. Gas geochemistry and CO2 output estimation at the island of Milos, Greece. J. Volcanol. Geotherm. Res. 365, 13–22. https://doi.org/10.1016/j.jvolgeores.2018.10.003.

Dibacto, S., Lahitte, P., Karátson, D., Hencz, M., Szakács, A., Biró, T., Kovács, I., Veres, D., 2020. Growth and erosion rates of the East Carpathians volcanoes constrained by numerical models: tectonic and climatic implications. Geomorphology 368, 107352. https://doi.org/10.1016/j.geomorph.2020.107352.

Downes, H., Seghedi, I., Szakács, A., Dobosi, G., James, D.E., Vaselli, O., Rigby, I.J., Ingram, G.A., Rex, D., Pécskay, Z., 1995. Petrology and geochemistry of late Tertiary/Quaternary mafic alkaline volcanism in Romania. Lithos 35, 65–81. https://doi.org/10.1016/0024-4937(95)91152-Y.

Dunai, T.J., Porcelli, D., 2002. Storage and transport of noble gases in the subcontinental lithosphere. Rev. Mineral. Geochem. 47 (1), 371–409. https://doi.org/10.2138/rmg.2002.47.10.

Faccini, B., Rizzo, A.L., Bonadiman, C., Ntaflos, T., Seghedi, I., Grégoire, M., Ferretti, G., Coltorti, M., 2020. Subduction-related melt refertilisation and alkaline metasomatism in the Eastern Transylvanian Basin lithospheric mantle: evidence from mineral chemistry and noble gases in fluid inclusions. Lithos 364-365, 105516. https://doi.org/10.1016/j.lithos.2020.105516.

Falus, G., Tommasi, A., Ingrin, J., Szabó, C., 2008. Deformation and seismic anisotropy of the lithospheric mantle in the southeastern Carpathians inferred from the study of mantle xenoliths. Earth Planet. Sci. Lett. 272, 50–64. https://doi.org/10.1016/j.epsl.2008.04.035.

Farley, K.A., 2002. (U-Th)/He dating: techniques, calibrations, and applications. Rev. Mineral. Geochem. 47 (1), 819–844. https://doi.org/10.2138/rmg.2002.47.18.

Graham, D.W., 2002. Noble gas isotope geochemistry of mid-ocean ridge and ocean island basalts: characterization of mantle source reservoirs. Rev. Mineral. Geochem. 47 (1), 247–317. https://doi.org/10.2138/rmg.2002.47.8.

Graham, D.W., Allard, P., Kilburn, C.R.J., Spera, F.J., Lupton, J.E., 1993. Helium isotopes in some historical lavas from Mount Vesuvius. J. Volcanol. Geotherm. Res. 58, 359–366. https://doi.org/10.1016/0377-0273(93)90117-A.

Hanyu, T., Kaneoka, I., 1997. Magmatic processes revealed by noble gas signatures: the case of Unzen Volcano, Japan. Geochem. J. 31, 395–405.

Harangi, S., Lenkey, L., 2007. Genesis of the Neogene to Quaternary volcanism in the Carpathian-Pannonian region: role of subduction, extension, and mantle plume. GSA Spec. Pap. 418, 67–92. https://doi.org/10.1130/2007.2418(04).

Harangi, S., Molnár, M., Vinkler, A.P., Kiss, B., Jull, A.J.T., Leonard, A.G., 2010. Radiocarbon dating of the last volcanic eruptions of Ciomadul volcano, Southeast Carpathians, Eastern-Central Europe. Radiocarbon 52 (2–3), 1498–1507. https://doi.org/10.1017/S0033822200046580.

Harangi, S., Sági, T., Seghedi, I., Ntaflos, T., 2013. Origin of basaltic magmas of Perşani volcanic field, Romania: a combined whole rock and mineral scale investigation. Lithos 180–181, 43–57. https://doi.org/10.1016/j.lithos.2013.08.025.

Harangi, S., Lukács, R., Schmitt, A.K., Dunkl, I., Molnár, K., Kiss, B., Seghedi, I., Novothny, Á., Molnár, M., 2015a. Constraints on the timing of Quaternary volcanism and duration of magma residence at Ciomadul volcano, east–central Europe, from combined U–Th/He and U–Th zircon geochronology. J. Volcanol. Geotherm. Res. 301, 66–80. https://doi.org/10.1016/j.jvolgeores.2015.05.002.

Harangi, S., Novák, A., Kiss, B., Seghedi, I., Lukács, R., Szarka, L., Wesztergom, V., Metwaly, M., Gribovszki, K., 2015b. Combined magnetotelluric and petrologic constrains for the nature of the magma storage system beneath the Late Pleistocene Ciomadul volcano (SE Carpathians). J. Volcanol. Geotherm. Res. 290, 82–96. https://doi.org/10.1016/j.jvolgeores.2014.12.006.

Harangi, S., Molnár, K., Schmitt, A.K., Dunkl, I., Seghedi, I., Novothny, Á., Molnár, M., Kiss, B., Ntaflos, T., Mason, P.R.D., Lukács, R., 2020. Fingerprinting the Late Pleistocene tephras of Ciomadul volcano, eastern-central Europe. J. Quat. Sci. 35 (1–2), 232–244. https://doi.org/10.1002/jqs.3177.

Hilton, D.R., Hoogewerff, J.A., van Bergen, M.J., Hammerschmidt, K., 1992. Mapping magma sources in the east Sunda-Banda arcs, Indonesia: constraints from helium isotopes. Geochm. Cosmochim. Acta 56, 851–859. https://doi.org/10.1016/0016-7037(92)90105-R.

Hilton, D.R., Hammerschmidt, K., Teufel, S., Friedrichsen, H., 1993. Helium isotope characteristics of Andean geothermal fluids and lavas. Earth Planet. Sci. Lett. 120, 265–282. https://doi.org/10.1016/0012-821X(93)90244-4.

Hilton, D.R., Fischer, T.P., Marty, B., 2002. Noble gases and volatile recycling at subduction zones. Rev. Mineral. Geochem. 47 (1), 319–370. https://doi.org/10.2138/rmg.2002.47.9.

Ianovici, V., Rădulescu, D., 1966. Geologicalmap 1:200000 L-35-XIV, Sheet 20 Odorhei. Geological Institute of Romania, Bucharest.

Karátson, D., Tímár, G., 2005. Comparative volumetric calculations of two segments of the Neogene/Quaternary volcanic chain using SRTM elevation data: implications for erosion and magma output rates. Z. Geomorphol. Suppl. 140, 19–35.

Karátson, D., Telbisz, T., Harangi, S., Magyari, E., Dunkl, I., Kiss, B., Jánosi, C., Veres, D., Braun, M., Fodor, E., Biró, T., Kósik, S., von Eynatten, H., Lin, D., 2013. Morphometrical and geochronological constraints on the youngest eruptive activity in East-Central Europe at the Ciomadul (Csomád) lava dome complex, East Carpathians. J. Volcanol. Geotherm. Res. 255 (0), 43–56. https://doi.org/10.1016/j.jvolgeores.2013.01.013.

Karátson, D., Wulf, S., Veres, D., Magyari, E.K., Gertisser, R., Timar-Gabor, A., Novothny, Á., Telbisz, T., Szalai, Z., Anechitei-Deacu, V., Appelt, O., Bormann, M., Jánosi, C., Hubay, K., Schäbitz, F., 2016. The latest explosive eruptions of Ciomadul (Csomád) volcano, East Carpathians — a tephrostratigraphic approach for the 51–29 ka BP time interval. J. Volcanol. Geotherm. Res. 319, 29–51. https://doi.org/10.1016/j.jvolgeores.2016.03.005.

Kis, B.M., Ionescu, A., Cardellini, C., Harangi, S., Baciu, C., Caracausi, A., Viveiros, F., 2017. Quantification of carbon dioxide emissions of Ciomadul, the youngest volcano of the Carpathian-Pannonian Region (Eastern-Central Europe, Romania). J. Volcanol. Geotherm. Res. 341, 119–130. https://doi.org/10.1016/j.jvolgeores.2017.05.025.

Kis, B.M., Caracausi, A., Palcsu, L., Baciu, C., Ionescu, A., Futó, I., Sciarra, A., Harangi, S., 2019. Noble gas and carbon isotope systematics at the seemingly inactive Ciomadul Volcano (eastern-central Europe, Romania): evidence for volcanic degassing. Geochem. Geophys. Geosyst. 20, 3019–3043. https://doi.org/10.1029/2018GC008153.

Kiss, B., Harangi, S., Ntaflos, T., Mason, P.R.D., Pál-Molnár, E., 2014. Amphibole perspective to unravel pre-eruptive processes and conditions in volcanic plumbing systems beneath intermediate arc volcanoes: a case study from Ciomadul volcano (SE Carpathians). Contrib. Mineral. Petrol. 167 (3), 1–27. https://doi.org/10.1007/s00410-014-0986-6.

Lahitte, P., Dibacto, S., Karátson, D., Gertisser, R., Veres, D., 2019. Eruptive history of the Late Quaternary Ciomadul (Csomád) volcano, East Carpathians, part I: timing of lava dome activity. Bull. Volcanol. 81, 27. https://doi.org/10.1007/s00445-019-1286-9.

Laumonier, M., Karakas, O., Bachmann, O., Gaillard, F., Lukács, R., Seghedi, I., Menand, T., Harangi, S., 2019. Evidence for a persistent magma reservoir with large melt content beneath an apparently extinct volcano. Earth Planet. Sci. Lett. 521, 79–90. https://doi.org/10.1016/j.epsl.2019.06.004.

Martelli, M., Nuccio, P.M., Stuart, F.M., Burgess, R., Ellam, R.M., Italiano, F., 2004. Helium–strontium isotope constraints on mantle evolution beneath the Roman Comagmatic Province, Italy. Earth Planet. Sci. Lett. 224, 295–308. https://doi.org/10.1016/j.epsl.2004.05.025.

Martin, M., Wenzel, F., Calixto, W.G., 2006. High-resolution teleseismic body wave tomography beneath SE-Romania – II. Imaging of a slab detachment scenario. Geophys. J. Int. 164 (3), 579–595. https://doi.org/10.1111/j.1365-246X.2006.02884.x.

Marty, B., Trull, T., Lussiez, P., Basile, I., Tanguy, J.C., 1994. He, Ar, O, Sr and Nd isotope constraints on the origin and evolution of Mount Etna magmatism. Earth Planet. Sci. Lett. 126, 23–39. https://doi.org/10.1016/0012-821X(94)90240-2.

Mason, P.R.D., Downes, H., Thirlwall, M., Seghedi, I., Szakács, A., Lowry, D., Mattey, D., 1996. Crustal assimilation as a major petrogenetic process in east Carpathian Neogene to Quaternary continental margin arc magmas. J. Petrol. 37, 927–959. https://doi.org/10.1093/petrology/37.4.927.

Molnár, K., Harangi, S., Lukács, R., Dunkl, I., Schmitt, A.K., Kiss, B., Garamhegyi, T., Seghedi, I., 2018. The onset of the volcanism in the Ciomadul Volcanic Dome Complex (Eastern Carpathians): Eruption chronology and magma type variation. J. Volcanol. Geotherm. Res. 354, 39–56. https://doi.org/10.1016/j.jvolgeores.2018.01.025.

Molnár, K., Lukács, R., Dunkl, I., Schmitt, A.K., Kiss, B., Seghedi, I., Szepesi, J., Harangi, S., 2019. Episodes of dormancy and eruption of the Late Pleistocene Ciomadul volcanic complex (Eastern Carpathians, Romania) constrained by zircon geochronology. J. Volcanol. Geotherm. Res. https://doi.org/10.1016/j.jvolgeores.2019.01.025.

Moriya, I., Okuno, M., Nakamura, E., Szakács, A., Seghedi, I., 1995. Last eruption and its 14C age of Ciomadul volcano, Romania. Summaries of Researches Using AMS at Nagoya University. 6, 82–91.

Moriya, I., Okuno, M., Nakamura, T., Ono, K.A.S., Seghedi, I., 1996. Radiocarbon ages of charcoal fragments from the pumice flow deposits of the last eruption of Ciomadul volcano, Romania. Summaries of Researches Using AMS at Nagoya University. VII (3), pp. 252–255.

Nuccio, P.M., Paonita, A., Rizzo, A., Rosciglione, A., 2008. Elemental and isotope covariation of noble gases in mineral phases from Etnean volcanics erupted during 2001–2005, and genetic relation with peripheral gas discharges. Earth Planet. Sci. Lett. 272 (3–4), 683–690. https://doi.org/10.1016/j.epsl.2008.06.007.

Osawa, T., 2004. A new correction technique for mass interferences by Ar^{++} and CO_2^{++} during isotope analysis of a small amount of Ne. J. Mass Spectrometry Soc. Japan 52 (4), 230–232. https://doi.org/10.5702/massspec.52.230.

Ozima, M., Podosek, F.A., 2004. Noble Gas Geochemistry. Cambridge University Press, Cambridge.

Panaiotu, C.G., Jicha, B.R., Singer, B.S., Ţugui, A., Seghedi, I., Panaiotu, A.G., Necula, C., 2013. 40Ar/39Ar chronology and paleomagnetism of Quaternary basaltic lavas from the Persani Mountains (East Carpathians). Phys. Earth Planet. Inter. 221, 1–14. https://doi.org/10.1016/j.gca.2012.01.028.

Paonita, A., Caracausi, A., Iacono-Marziano, G., Martelli, M., Rizzo, A., 2012. Geochemical evidence for mixing between fluid exsolved at different depths in the magmatic system of Mt Etna (Italy). Geochim. Cosmochim. Acta 84, 380–394.

Papp, L., Palcsu, L., Major, Z., Rinyu, L., Tóth, I., 2012. A mass spectrometric line for tritium analysis of water and noble gas measurements from different water amounts in the range of microlitres and millilitres. Isot. Environ. Health Stud. 48 (1), 494–511. https://doi.org/10.1080/10256016.2012.679935.

Pécskay, Z., Lexa, J., Szakács, A., Balogh, K., Seghedi, I., Konecny, V., Kovács, M., Márton, E., Kaliciak, M., Széky-Fux, V., Póka, T., Gyarmati, P., Edelstein, O., Rosu, E., Zec, B., 1995. Space and time distribution of Neogene-Quaternary volcanism in the Carpatho-Pannonian Region. In: Downes, H., Vaselli, O. (Eds.), Neogene and Related Magmatism in the Carpatho-Pannonian Region. Acta Vulcanologica, pp. 15–28.

Pécskay, Z., Lexa, J., Szakács, A., Seghedi, I., Balogh, K., Konecný, V., Zelenka, T., Kovacs, M., Póka, T., Fülöp, A., Márton, E., Panaiotu, C., Cvetkovic, V., 2006. Geochronology of Neogene magmatism in the Carpathian arc and intra-Carpathian area. Geol. Carpath. 57 (6), 511–530.

Pik, R., Marty, B., 2009. Helium isotopic signature of modern and fossil fluids associated with the Corinth rift fault zone (Greece): Implication for fault connectivity in the lower crust. Chem. Geol. 266 (1–2), 67–75. https://doi.org/10.1016/j.chemgeo.2008.09.024.

Popa, M., Radulian, M., Szakács, A., Seghedi, I., Zaharia, B., 2012. New seismic and tomography data in the southern part of the Harghita mountains (Romania, Southeastern Carpathians): connection with recent volcanic activity. Pure Appl. Geophys. 169 (9), 1557–1573. https://doi.org/10.1007/s00024-011-0428-6.

Rizzo, A.L., Barbieri, F., Carapezza, M.L., Di Piazza, A., Francalanci, L., Sortino, F., D'Alessandro, W., 2015. New mafic magma refilling a quiescent volcano: evidence from He-Ne-Ar isotopes during the 2011–2012 unrest at Santorini, Greece. Geochem. Geophys. Geosyst. 16, 798–814. https://doi.org/10.1002/2014GC005653.

Rizzo, A.L., Caracausi, A., Chavagnac, V., Nomikou, P., Polymenakou, P.N., Mandalakis, M., Kotoulas, G., Magoulas, A., Castillo, A., Lampridou, D., 2016. Kolumbo submarine volcano (Greece): an active window into the Aegean subduction system. Sci. Rep. 6, 28013. https://doi.org/10.1038/srep28013.

Robidoux, P., Rizzo, A.L., Aguilera, F., Aiuppa, A., Artale, M., Liuzzo, M., Nazzari, M., Zummo, F., 2020. Petrological and noble gas features of Lascar and Lastarria volcanoes (Chile): inferences on plumbing systems and mantle characteristics. Lithos 370–371, 105615. https://doi.org/10.1016/j.lithos.2020.105615.

Sano, Y., Marty, B., 1995. Origin of carbon in fumarolic gas from island arcs. Chem. Geol. 119 (1–4), 265–274. https://doi.org/10.1016/0009-2541(94)00097-R.

Sano, Y., Wakita, H., 1985. Geographical distribution of 3He/4He ratios in Japan: implications for arc tectonics and incipient magmatism. J. Geophys. Res. 90, 8729–8741. https://doi.org/10.1029/JB090iB10p08729.

Sano, Y., Wakita, H., Italiano, F., Nuccio, M.P., 1989. Helium isotopes and tectonics in southern Italy. Geophys. Res. Lett. 16 (6), 511–514. https://doi.org/10.1029/GL016i006p00511.

Sano, Y., Marty, B., Burnard, P., 2013. Noble gases in the atmosphere. In: Burnard, P. (Ed.), The Noble Gases as Geochemical Tracers. Advances in Isotope Geochemistry. Springer, pp. 17–31 https://doi.org/10.1007/978-3-642-28836-4_2.

Sano, Y., Kagoshima, T., Takahata, N., Nishio, Y., Roulleau, E., Pinti, D.L., Fischer, T.P., 2015. Ten-year helium anomaly prior to the 2014 Mt. Ontake eruption. Sci. Rep. 5, 13069. https://doi.org/10.1038/srep13069.

Schafarzik, F., 1904. A Magyar Korona országai területén létező kőbányák részletes ismertetése. Magyar Királyi Földtani Intézet, p. 487 (in Hungarian).

Seghedi, I., Downes, H., Szakács, A., Mason, P.R.D., Thirlwall, M.F., Roșu, E., Pécskay, Z., Márton, E., Panaiotu, C., 2004. Neogene-Quaternary magmatism and geodynamics in the Carpathian-Pannonian region: a synthesis. Lithos 72, 117–146. https://doi.org/10.1016/j.lithos.2003.08.006.

Seghedi, I., Maţenco, L., Downes, H., Mason, P.R.D., Szakács, A., Pécskay, Z., 2011. Tectonic significance of changes in post-subduction Pliocene–Quaternary magmatism in the south east part of the Carpathian–Pannonian Region. Tectonophysics 502 (1–2), 146–157. https://doi.org/10.1016/j.tecto.2009.12.003.

Seghedi, I., Besutiu, L., Mirea, V., Zlagnean, L., Popa, R.G., Szakács, A., Atanasiu, L., Pomeran, M., Vişan, M., 2019. Tectono-magmatic characteristics of post-collisional magmatism: Case study East Carpathians, Călimani-Gurghiu-Harghita volcanic range. Phys. Earth Planet. Inter. 293, 106270. https://doi.org/10.1016/j.pepi.2019.106270.

Szakács, A., Seghedi, I., 1987. Base surge deposits in the Ciomadul Massif (South Harghita Mountains). D.S. Inst. Geol. Geofiz 74 (1), 175–180.

Szakács, A., Seghedi, I., 1995. The Călimani-Gurghiu-Harghita volcanic chain, East Carpathians, Romania: volcanological features. Acta Vulcanol. 7 (2), 145–153.

Szakács, A., Seghedi, I., Pécskay, Z., 1993. Pecularities of South Hargita Mts. as the terminal segment of the Carpathian Neogene to Quaternary volcanic chain. Rev. Roumaine Geol. Geophys. Geogr. Geol. 37, 21–37.

Szakács, A., Seghedi, I., Pécskay, Z., Mirea, V., 2015. Eruptive history of a low-frequency and low-output rate Pleistocene volcano, Ciomadul, South Harghita Mts., Romania. Bull. Volcanol. 77 (2), 1–19. https://doi.org/10.1007/s00445-014-0894-7.

Vaselli, O., Downes, H., Thirwall, M., Dobosi, G., Coradossi, N., Seghedi, I., Szakacs, A., Vannucci, R., 1995. Ultramafic Xenoliths in Plio-Pleistocene Alkali Basalts from the Eastern Transylvanian Basin: Depleted Mantle Enriched by Vein Metasomatism. J. Petrol. 36 (1), 23–53. https://doi.org/10.1093/petrology/36.1.23.

Vaselli, O., Minissale, A., Tassi, F., Magro, G., Seghedi, I., Ioane, D., Szakács, A., 2002. A geochemical traverse across the Eastern Carpathians (Romania): constraints on the origin and evolution of the mineral water and gas discharges. Chem. Geol. 182, 637–654. https://doi.org/10.1016/S0009-2541(01)00348-5.

Vinkler, A.P., Harangi, S., Ntaflos, T., Szakács, A., 2007. Petrology and geochemistry of the pumices from the Ciomadul volcano (Eastern Carpathians) – implications for the petrogenetic processes. Földtani Közlöny 137 (1), 103–128 (In Hungarian).